Structure of the Agonist-Binding Sites of the *Torpedo* Nicotinic Acetylcholine Receptor: Affinity-Labeling and Mutational Analyses Identify γTyr-111/δArg-113 as Antagonist Affinity Determinants†

David C. Chiara,‡ Yu Xie,‡,§ and Jonathan B. Cohen*

Department of Neurobiology, Harvard Medical School, Boston, Massachusetts 02115

Received January 25, 1999; Revised Manuscript Received March 18, 1999

ABSTRACT: Photoaffinity labeling of the *Torpedo* nicotinic acetylcholine receptor (nAChR) with [^{3}H]*d*-tubocurarine (dTC) has identified a residue within the γ-subunit which, along with the analogous residue in δ-subunit, confers selectivity in binding affinities between the two agonist sites for dTC and α-conotoxin (αCtx) MI. nAChR γ-subunit, isolated from nAChR-rich membranes photolabeled with [^{3}H]dTC, was digested with *Staphylococcus aureus* V8 protease, and a ^{3}H-labeled fragment was purified by reversed-phase high-performance liquid chromatography. Amino-terminal sequence analysis of this fragment identified ^{3}H incorporation in γTyr-111 and γTyr-117 at about 5% and 1% of the efficiency of [^{3}H]dTC photoincorporation at γTrp-55, the primary site of [^{3}H]dTC photoincorporation within γ-subunit [Chiara, D. C., and Cohen, J. B. (1997) *J. Biol. Chem 272*, 32940−32950]. The *Torpedo* nAChR δ-subunit residue corresponding to γTyr-111 (δArg-113) contains a positive charge which could confer the lower binding affinity seen for some competitive antagonists at the α−δ agonist site. To test this hypothesis, we examined by voltage-clamp analysis and/or by [^{125}I]α-bungarotoxin competition binding assays the interactions of acetylcholine (ACh), dTC, and αCtx MI with nAChRs containing γY111R or δR113Y mutant subunits expressed in *Xenopus* oocytes. While these mutations affected neither ACh equilibrium binding affinity nor the concentration dependence of channel activation, the γY111R mutation decreased by 10-fold dTC affinity and inhibition potency. Additionally, each mutation conferred a *1000-fold* change in the equilibrium binding of αCtx MI, with δR113Y enhancing and γY111R weakening affinity. Comparison of these results with previous results for mouse nAChR reveals that, while the same regions of γ- (or δ-) subunit primary structure contribute to the agonist-binding sites, the particular amino acids that serve as antagonist affinity determinants are species-dependent.

The *Torpedo* nicotinic acetylcholine receptor (nAChR[1]) is a ligand-gated ion channel composed of 4 homologous membrane-spanning subunits arranged as a pentamer ($\alpha_2\beta\gamma\delta$) around a central channel. Considerable structural information about the nAChR is known from affinity-labeling studies, site-directed mutational analyses, and a low-resolution (9 Å) cryoelectron microscopy structure (for review, see refs *1*−*4*). The two ACh-binding sites, which are located extracellularly at the α−γ- and α−δ-subunit interfaces, are composed of multiple loops of primary structure from both the α- and non-α-subunits. Many competitive antagonists bind to the two agonist sites nonequivalently. For example, in *Torpedo* nAChR, *d*-tubocurarine (dTC) and α-conotoxin (αCtx) MI bind to the α−γ site with 200- and 600-fold higher affinity than to the α−δ site, respectively (*5*−*7*). However these site selectivities are species-specific, since, in mouse embryonic nAChR, dTC binds with only 10-fold higher affinity to the α−γ site, while αCtx MI actually binds with 3000-fold higher affinity to the α−δ site (*7*, *8*). These differences in binding affinities between agonist sites are likely to reflect contributions from the non-α-subunits, since the 2 α-subunits in either *Torpedo* or mouse nAChR should be essentially identical (but see refs *9*, *10*). For mouse muscle nAChR, γ-subunit residues 116, 117, and 161 (and the corresponding residues in δ) together confer the affinity differences between the two agonist sites for metocurarine and other dTC analogues (*11*). Additionally, γ-subunit residues 34, 111, and 172 (together) and the corresponding δ-subunit residues confer the nonequivalent binding affinities of αCtx MI for mouse muscle nAChR (*12*).

UV irradiation of *Torpedo* nAChR-rich membranes equilibrated with [^{3}H]dTC results in covalent incorporation of [^{3}H]-

† This research was supported in part by USPHS Grant NS 19522 and by an award in Structural Neurobiology by the Keck Foundation. D.C.C. was supported in part by Training Grant GM-07809 (to Washington University School of Medicine), and Y.X. was a Harvard Mahoney Neuroscience Institute fellow.

* To whom correspondence should be addressed: Department of Neurobiology, Harvard Medical School, 220 Longwood Avenue, Boston, MA. 02115. Tel: (617) 432-1728. Fax: (617) 734-7557. Email: jonathan_cohen@hms.harvard.edu.

‡ These authors contributed equally to this work.

§ Present address: Millennium Pharmaceuticals, Inc., Cambridge, MA., 02139-4815, USA.

[1] Abbreviations: nAChR, nicotinic acetylcholine receptor; dTC, *d*-tubocurarine; αCtx, α-conotoxin; V8 protease, *Staphylococcus aureus* glutamyl endopeptidase; Endo H, endo-β-*N*-acetylglucosaminidase H; ACh, acetylcholine; αBtx, α-bungarotoxin; Carb, carbamylcholine; *N*-acetylglucosaminylasparagine, 2-acetamido-1-*N*-(β-L-aspartyl)-2-deoxy-β-D-glucopyranosylamine; SDS−PAGE, sodium dodecyl sulfate−polyacrylamide gel electrophoresis; HPLC, high-performance liquid chromatography.

10.1021/bi9901735 CCC: $18.00
Published on Web 04/29/1999

dTC into the nAChR α-, γ-, and δ-subunits in an agonist-inhibitable and concentration-dependent manner (*13*). Within α-subunit the primary site of [^{3}H]dTC labeling is at Tyr-190, with additional incorporation at Cys-192 and Tyr-198 (*14*). Incorporation into the two other α-subunit regions contributing to the agonist-binding sites (near αTyr-93 and αTrp-149 (*15*−*17*)) is not detected (i.e., <2% the efficiency of incorporation in αTyr-190). The efficiency of specific [^{3}H]-dTC photoincorporation within the γ- and δ-subunits was similar to that for α-subunit, with the primary sites of incorporation at homologous tryptophans, γTrp-55 and δTrp-57 (*14*). There was no detectable [^{3}H]dTC incorporation in the δ-subunit region near δAsp-180 identified by chemical cross-linking from αCys-192 (*18*). Although mutational analyses of γTrp-55 and δTrp-57 reveal their considerable importance in agonist binding and channel activation (*19*, *20*), these tryptophans are not important determinants of dTC affinity and cannot account for the difference in antagonist-binding affinities between the two agonist sites of the *Torpedo* nAChR.

We report here the identification of γTyr-111 and γTyr-117 as additional amino acids within the γ-subunit that are specifically photolabeled by [^{3}H]dTC. As with γTrp-55, [^{3}H]-dTC photoincorporation at these positions is inhibited by agonist, but the efficiency of photoincorporation is only 5% of that of γTrp-55. By comparing functional properties of mutant nAChRs containing γY111R or δR113Y, we establish that this position does not play an important role in agonist binding, but it is a major determinant of the selective high-affinity binding of dTC and αCtx MI at the α−γ site in the *Torpedo* nAChR. In fact, replacement of a single amino acid in γ- (γY111R) or in δ-subunit (δR113Y) confers a reversal in the site specificity for αCtx MI.

EXPERIMENTAL PROCEDURES

Materials. nAChR-rich membranes, prepared from *Torpedo californica* electric organ (Marinus, Westchester, CA) as described (*21*) and stored in 38% sucrose/0.02% NaN_3 at −80 °C, contained ∼1.5 nmol of [^{3}H]acetylcholine (ACh) sites per milligram of protein. [^{3}H]dTC was prepared as described (*13*) at a radiochemical specific activity of 30 Ci/mmol. SP64T-based plasmids (pMXT) with cDNAs encoding *Torpedo* nAChR α-, γ-, δ-subunits were gifts from Dr. Michael White (Allegheny Health Science University), and the cDNA (in plasmid SP64) encoding the *Torpedo* nAChR β-subunit was from Dr. Henry Lester (California Institute of Technology). [^{125}I]α-Bungarotoxin (αBtx, 400−600 Ci/mmol) was prepared using Iodogen (Pierce) as described in ref *22*. α-Bungarotoxin was from Biotoxins Incorporated. Carbamylcholine (Carb), 2-acetamido-1-*N*-(β-L-aspartyl)-2-deoxy-β-D-glucopyranosylamine (*N*-acetylglucosaminylasparagine), acetylcholine, *d*-tubocurarine, and α-conotoxin MI were from Sigma.

Methods

Photolabeling of nAChR−Rich Membranes with [^{3}H]dTC. nAChR-rich membranes (10 mg, 9−17 nmol of ACh-binding sites in 8 mL of 250 mM NaCl, 5 mM KCl, 3 mM $CaCl_2$, 2 mM $MgCl_2$, and 5 mM sodium phosphate, pH 7.0) equilibrated with [^{3}H]dTC (0.5−2 μM) were exposed to 254 nm UV light for 5 min as described in ref *14*. Carb (1 mM) was added to parallel membrane samples prior to photolysis to define nonspecific photolabeling. Oxidized glutathione (500 μM) was included as an aqueous photochemical scavenger in all samples. The polypeptides of the photolabeled nAChR-rich membranes were separated by sodium dodecyl sulfate−polyacrylamide gel electrophoresis (SDS−PAGE), and γ-subunit was excised and either eluted from the gel pieces as described in ref *14* or placed on a second, mapping gel for "in gel" digestion (see below).

Isolation of [^{3}H]dTC-Labeled γ-Subunit Fragments. Solution digests with *Staphylococcus aureus* glutamyl endopeptidase (V8-protease, Boehringer Mannheim), endo-β-*N*-acetylglucosaminidase H (Endo H, Genzyme), or *N*-Glycanase (Genzyme) were performed at 25 °C in 10 mM sodium phosphate buffer, pH 7.0, with 1 mM DTT, 1 mM EDTA, and 0.1% SDS (storage buffer) with the addition of 0.5% Lubrol-PX (Pierce) for *N*-Glycanase-treated samples. Enzyme concentrations and incubation times are indicated in the figure legends. ^{3}H-labeled γ-subunit was also digested with *S. aureus* V8-protease (ICN Biochemical) by the "in gel" method of Cleveland (*23*), and fragments of interest were identified and eluted from the gels as described in ref *14*. Reversed-phase HPLC was performed on system components as described in ref *24* using a Brownlee Aquapore C_4 column (220 mm × 2.1 mm). Elution solvents and conditions are described in the figure legends. Deglycosylated γ-subunit fragments were separated by SDS−PAGE using the tricine gel system of Schägger and von Jagow (*25*), with subsequent ^{3}H detection achieved by fluorography of Enh^3-ance (Dupont)-treated gels. Molecular mass standards used for analytical SDS−PAGE were the following: carbonic anhydrase (29 kDa), soybean trypsin inhibitor (20.1 kDa), and cytochrome C (12.4 kDa).

Amino-Terminal Sequence Analysis. An Applied Biosystems Model 470A protein sequencer with an inline Model 120A PTH-amino acid analyzer was used to sequence samples of interest. Approximately 40% of each cycle was injected into the 120A for amino acid mass analysis, while 40% was collected for ^{3}H determination by liquid scintillation counting. The actual counts per minute and picomoles detected are reported. Pooled HPLC fractions of interest were dried by vacuum centrifugation and resuspended in a small volume of storage buffer (50−100 μL). Aliquots (up to 120 μL) of samples in storage buffer were loaded directly onto trifluoroacetic acid-treated glass-fiber filters coated with 3 mg of Polybrene for sequence analysis. Cycle yields for PTH-amino acids were estimated from peak heights. Initial peptide mass (*I*) and repetitive yield (*R*) were calculated by nonlinear least-squares regression (Sigma Plot) of the function $f(x) = IR^x$ where $f(x)$ is the observed mass released in cycle x. PTH derivatives of Ser, Cys, Arg, His, and Trp were excluded from the fits due to known problems with measuring mass yields of these residues. In some cases, sequencing of nonrelevant peptides was blocked by treatment of the sample on the filter with *o*-phthalaldehyde (Pierce). *o*-Phthalaldehyde reacts with primary, but not secondary, amines and can be used to block Edman degradation of any peptide not containing an N-terminal proline (*26*). *o*-Phthalaldehyde treatment was carried out as described (*21*).

In Vitro Transcription and Expression in Xenopus Oocytes. cDNAs were linearized with either *Xba*I (for α-, γ-, and δ-subunits) or *Fsp*I (for β-subunit). Linear cDNAs (5−10

μg) were transcribed in vitro using SP6 RNA polymerase (Promega). In some experiments, [^{3}H]UTP (Andotek) was included in the reaction mixture as a tracer for quantitation of reaction yields. RNAs were extracted with phenol/chloroform and chloroform, precipitated from 2-propanol, and then resuspended in water at a concentration of ~3 μg/μL. Isolated follicle-free oocytes were microinjected with a mixture of subunit-specific RNAs in molar stoichiometries of ($\alpha_2\beta\gamma\delta$) for wild-type and mutant receptors, ($\alpha_2\beta\delta_2$) for γ-less receptors, and ($\alpha_2\beta\gamma_2$) for δ-less receptors. Oocytes were injected with 10 ng of subunit RNA mixtures for assays of [^{125}I]αBtx binding and for electrophysiological assays of dTC inhibition, or with 0.5 ng for full ACh-dose response measurements. Oocytes were maintained in ND96 buffer containing 96 mM NaCl, 2 mM KCl, 1.8 mM $CaCl_2$, 1 mM $MgCl_2$, 5 mM HEPES (pH 7.6), and 50 μg/mL gentamicin for at least 48 h before use.

Site-Directed Mutagenesis. Single-stranded cDNAs for γ- and δ-subunits were obtained using the helper phage VCSM13 (Stratagene) according to the supplier protocol. The point mutations γY111R and δR113Y were made by use of a commercially available kit (Mutagene M13, BIO-RAD). Mutagenic primers were 20−25 nucleotides in length, with the mismatched base(s) in the middle of the sequence. γY111R and δR113Y mutations were confirmed by DNA sequencing.

Preparation of Oocyte Membranes. Oocyte membranes were prepared by homogenizing injected oocytes in ice-cold homogenization buffer (HB, 0.1 mL/oocyte) containing 140 mM NaCl, 20 mM sodium phosphate, 1 mM EDTA, 1 mM EGTA, 1 mM PMSF, and 0.1 unit/mL Aprotinin (pH 7.6). Homogenates were centrifuged for 10 min at 800*g*, the supernatants were saved, and the pellets were resuspended in HB buffer and pelleted again. The combined supernatants were layered over 4 mL of 15% (wt/vol) sucrose and centrifuged at 4 °C in a Ti 70 rotor at 50 000 rpm for 1.2 h. The pellets were resuspended in HB at 5 μL per oocyte, frozen in liquid nitrogen, and stored at −80 °C (modified from ref *27*).

Binding of [^{125}I]αBtx. To measure binding to AChRs expressed on the surface, we incubated oocytes with 2.5 nM [^{125}I]αBtx for 2 h in a final volume of 0.1 mL of low-Ca^{2+} ND96 buffer. Oocytes were washed 3 times with 1 mL of ice-cold low- Ca^{2+} ND96 buffer containing 1% BSA and counted in a gamma counter. Nonspecific binding was determined using noninjected oocytes. Measurements of the initial rate of [^{125}I]αBtx binding to oocyte membranes were also carried out in low-Ca^{2+} ND96 assay buffer, supplemented with 0.1 mM diisopropylphosphofluoridate (DFP), a cholinesterase inhibitor, for ACh-binding experiments. Binding assays were initiated by adding [^{125}I]αBtx (a final concentration of 2.5 nM) to triplicate samples (membranes equivalent of 2−3 oocytes/sample), in a total volume of 100 μL. Membranes were pre-equilibrated with the appropriate concentrations of dTC or ACh for 15 min, or with αCtx-MI for 1 h prior to the addition of [^{125}I]αBtx. After 20 min, [^{125}I]αBtx binding was quenched by adding 1 μM αBtx. ([^{125}I]αBtx binds ~30% of the available αBtx-binding sites in 20 min.) The samples were pelleted at 150000*g* for 20 min, and the pellets were washed once with assay buffer and recentrifuged. After centrifugation, the supernatants were removed and the tubes were counted in a gamma counter. Nonspecific binding of [^{125}I]αBtx to wild-type and mutant receptors was determined in the presence of either 100 μM dTC (24% ± 6% of total binding, $N = 8$ experiments) or 100 mM ACh (27% ± 15% of total binding, $N = 8$ experiments) for dTC and ACh inhibition, respectively.

Electrophysiology. Currents elicited by ACh were measured using a standard two-electrode voltage clamp (Oocyte Clamp OC-725B, Warner Instrument Corp.) at a holding potential of −70 mV. Electrodes were filled with 3 M KCl and had resistances of 0.5−1.5 MΩ. The recording chamber (about 150 μL in volume) was perfused continually at 8 mL/min by gravity with low-Ca^{2+} ND96 (+1 μM atropine, pH 7.6). Appropriate concentrations of ACh in the absence or presence of dTC were applied through solenoid valves into the recording chamber for 3−5 s. Prior to application of ACh and dTC, oocytes were perfused with the appropriate concentration of dTC for 1 min.

Data Analysis. The concentration-dependent inhibition of [^{125}I]αBtx binding by agonists and antagonists was fit according to the two following models:

$$f(x) = 100/(1 + (x/IC_{50})^n) \quad (1)$$

and

$$f(x) = (50/(1 + (x/K_{dH}))) + (50/(1+(x/K_{dL}))) \quad (2)$$

where $f(x)$ is the [^{125}I]αBtx binding seen in the presence of inhibitor concentration x (as the percent of control), n is the Hill coefficient, IC_{50} is the inhibitor concentration reducing [^{125}I]αBtx binding by 50%, and K_{dH} and K_{dL} are the disassociation constants for the high- and low-affinity binding sites, respectively. Equation 2 is based on the assumption that αBtx binds at equal rates to the two sites. For receptor activation, concentration−response curves for ACh were fit to

$$f(x) = (1 + (K_{ap}/x)^n)^{-1} \quad (3)$$

where $f(x)$ is the percent of maximal current at ACh concentration x and K_{ap} is the apparent activation constant for ACh. The Hill coefficients (n_H) for the agonist dose−response relations were estimated from the slope of plots of log I vs log [agonist] at currents less than 20% of the maximal response for each agonist. The dose-dependent inhibition of ACh-induced currents by antagonists was fit according to eq 1 above using current instead of [^{125}I]αBtx binding. SigmaPlot (Jandel Scientific) was used for nonlinear least-squares fit of the data, and the standard errors of the parameter fits are indicated.

RESULTS

[^{3}H]d-Tubocurarine Photolabeling. Irradiation at 254 nm of nAChR-rich membranes equilibrated with [^{3}H]dTC results in agonist-inhibitable incorporation of ^{3}H into the α-, γ-, and δ-subunits, with γTrp-55 as the primary site of [^{3}H]-dTC photoincorporation in γ-subunit (*14*). To identify additional amino acids photolabeled by bound [^{3}H]dTC, we digested γ-subunit in solution with V8 protease. Fractionation of this digest by SDS−PAGE revealed a prominent ^{3}H band of 14 kDa (Figure 1 lanes A and B). This ^{3}H-labeled fragment contained an Asn-linked carbohydrate sensitive to

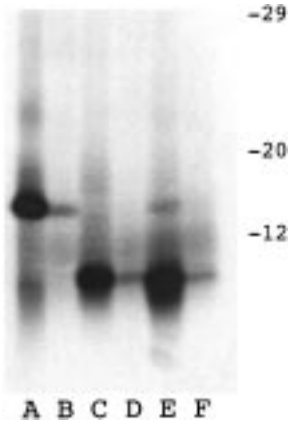

FIGURE 1: Digestion of [^{3}H]dTC-labeled nAChR γ-subunit by V8 protease produces a 14 kDa labeled fragment containing carbohydrate sensitive to Endo H. nAChR-rich membranes (11 mg, 13 nmol of ACh-binding sites) were photolabeled with 2 μM [^{3}H]dTC (±Carb), and labeled γ-subunit (−Carb, 2450 ^{3}H cpm/μg; +Carb, 1370 cpm/μg) was isolated by SDS−PAGE. Aliquots (8 μg) of γ-subunit (±Carb) were incubated overnight (25 °C) either without glycosidase (A and B), with 5 milliunits of Endo H (C and D), or with 0.5 units of *N*-Glycanase (E and F). The samples were then digested with V8 protease (50 μg for 3 h at 25 °C) and fractionated by SDS−PAGE (tricine gel, 8% T/3% C). The stained gel was treated with En^{3}hance for fluorography (−Carb, Lanes A, C, and E; +Carb, Lanes B, D, and F). The apparent molecular masses for the ^{3}H bands were 14 kDa for A and 8 kDa for C and E, as calculated from the mobilities of molecular mass markers.

Endo H (Figure 1, lanes C and D), which cleaves high mannose and some hybrid Asn-linked carbohydrates (*28*), and N-glycanase (Figure 1, lanes E and F), which cleaves all Asn-linked carbohydrates (*29*). This association of ^{3}H with an Endo H-sensitive carbohydrate in a 14 kDa band was in contrast to the result obtained after digestion of [^{3}H]dTC-labeled γ-subunit with V8 protease in gel, which resulted in a 14 kDa fragment beginning at γAla-49 containing an Asn-linked carbohydrate insensitive to Endo H (*14*).

To identify the [^{3}H]dTC-labeled fragment, samples of ^{3}H-labeled γ-subunit isolated from nAChRs labeled in the absence or presence of carbamylcholine were digested with V8 protease in solution and fractionated by HPLC (Figure 2A). For the sample labeled in the absence of agonist, in addition to ^{3}H recovered in the flow through (fraction 3), there was a single major peak of ^{3}H (fraction 6) containing twelve percent of injected ^{3}H. For each labeling condition, N-terminal sequence analysis of the material in this fraction identified a primary γ-subunit fragment beginning at γVal-102 (−Carb, I = 41 pmol; +Carb, I = 36 pmol). This primary sequence was present at a 4-fold higher level than a fragment beginning at γLeu-373 (−Carb, I = 10 pmol), and several fragments of V8 protease itself were also present at ∼10 pmol. For the sample labeled in the absence of agonist, there was a prominent peak of ^{3}H release (Figure 2B) in cycle 10 (190 cpm) with a minor peak in cycle 16 (20 cpm), consistent with [^{3}H]dTC labeling at γTyr-111 and γTyr-117. This labeling resulted from specific labeling of the agonist site, with incorporation at γTyr-111 reduced by >95% for the sample labeled in the presence of Carb.

To verify that the fragment beginning at γVal-102 was indeed the source of the ^{3}H release, we identified the glycosylation site contained within the ^{3}H-labeled 14 kDa fragment of Figure 1. Only two of the four consensus sites

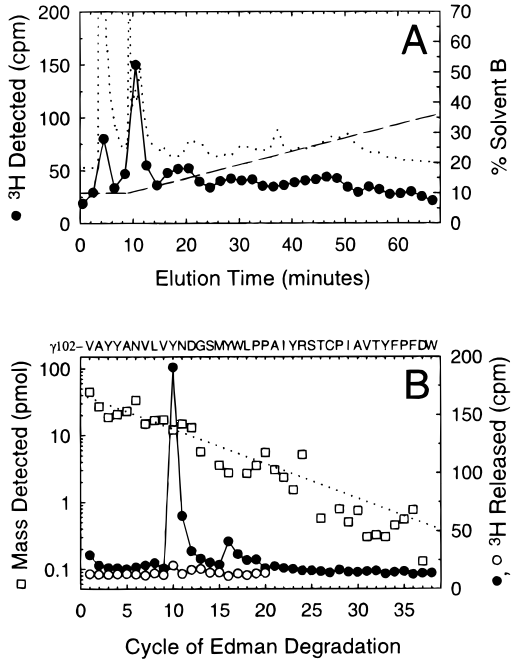

FIGURE 2: Purification and amino-terminal sequence analysis of [^{3}H]dTC-labeled γ-subunit fragment beginning at γVal-102. nAChR-rich membranes (10 mg, 17 nmol of ACh-binding sites) were photolabeled with 500 nM [^{3}H]dTC (±Carb), and labeled γ-subunits (−Carb, 930 cpm/μg; +Carb, 80 cpm/μg) were isolated by SDS−PAGE. Aliquots of γ-subunit (35 μg ±Carb) were digested with 10 μg of V8 protease for 2 weeks at 25 °C and then fractionated by reversed-phase HPLC on a C_4 column (flow rate of 0.25 mL/min). Solvent A was 0.1% TFA in 25% acetonitrile/75% water, and Solvent B was 0.1% TFA in 25% acetonitrile/75% isobutanol, with a gradient from 10% to 40% Solvent B in 67.5 min. (A) HPLC profile of −Carb sample (●, ^{3}H in 25 μL aliquots of 0.5 mL fractions (33 000 cpm loaded, 23 000 cpm recovered); (···), 280 nm absorbance; and (- - -), % Solvent B). The material in fraction 6 was concentrated and sequenced (as was the same fraction from the +Carb sample). (B) ^{3}H release profiles during Edman degradation (●, −Carb, 3000 cpm loaded, 600 cpm left after 38 cycles of Edman degradation; ○, +Carb, 500 cpm loaded, 200 cpm left after 20 cycles). Two γ-subunit fragments were detected beginning at γVal-102 (□, I = 46 pmol, R = 93%) and γLeu-372 (I = 10 pmol). The + Carb sample also contained fragments beginning at γVal-102 (I = 37 pmol, R = 89%) and γLeu-372 (I = 5 pmol). The dotted line represents a best fit of the mass values for the PTH-amino acids detected for the γVal-102 fragment (−Carb), calculated as described in Methods. Release of ^{3}H in cycle 10 (170 cpm) and cycle 16 (20 cpm) was consistent with agonist-inhibitable [^{3}H]dTC incorporation into γTyr-111 (13 cpm/pmol) and γTyr-117 (3 cpm/pmol).

for Asn-linked glycosylation in *Torpedo* nAChR γ-subunit (Asn-68, -141, -306, and -421) contain carbohydrate, one which is sensitive to Endo H, and one which is resistant to Endo H (*30*). To confirm that γAsn-141 was the Endo H-sensitive site associated with the [^{3}H]dTC-labeled residue, we sequenced through this position after Endo H treatment of a trypsin digest of γ-subunit. Trypsin cleavage of γ-subunit would generate a fragment beginning at γSer-126 containing two prolines (γPro-129 and 136) before γAsn-141 (Figure 3A). After treatment of the sample on the sequencing filter with *o*-phthalaldehyde prior to the fourth and eleventh cycles of Edman degradation to block the amino termini of peptides not containing prolines at those positions (*26*), the fragment beginning at γSer-126 was the only sequence detected (I = 42 pmol, data not shown). To determine whether Endo H did remove carbohydrate at γAsn-141, we took advantage

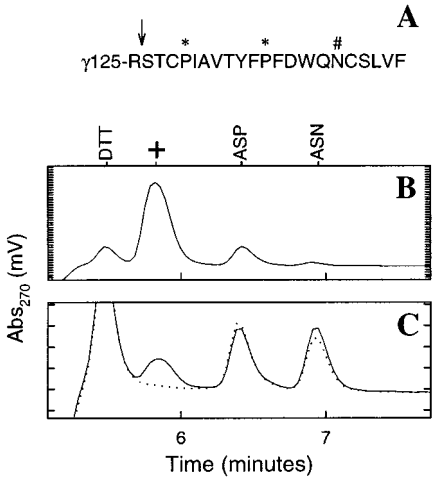

FIGURE 3: Identification of Endo H-sensitive oligosaccharide at nAChR γAsn-141. (A) Partial primary sequence of *Torpedo* nAChR γ-subunit denoting a trypsin cleavage site (↓), prolines (*), and the expected site of Asn-linked glycosylation (#). (B) HPLC retention time of the PTH derivative of 2-acetamido-1-*N*-(β-L-aspartyl)-2-deoxy-β-D-glucopyranosylamine (*N*-acetylglucosaminylasparagine). *N*-acetylglucosaminylasparagine (1 nmol in 30% acetonitrile) was applied to a sequencing filter and then converted to a PTH derivative, with the product analyzed on the sequencer PTH-amino acid analyzer. A novel peak corresponding to the PTH derivative of *N*-acetylglucosaminylasparagine (+) was seen between the dithiothreitol (DTT) and PTH-aspartate (ASP) peaks, consistent with the findings of Paxton et al. (*31*). Also indicated is the retention time of the PTH derivative of asparagine (ASN). (C) Consecutive chromatograms (cycles 15 and 16, dotted and solid lines, respectively) during sequence analysis of a trypsin digest of nAChR γ-subunit (150 μg, deglycosylated with Endo H, 10 milliunits, overnight as per Methods). After the third and tenth cycles of Edman degradation, the sample on the sequencing filter was treated manually with *o*-phthalaldehyde, which reacts selectively with the free amino termini of amino acids other than proline, a secondary amine, blocking Edman degradation (*26*). After the second treatment with *o*-phthalaldehyde, only a single sequence was detected, an nAChR γ-subunit fragment originating at γSer-126 (I = 42 pmol, R = 90%, 8 pmol in cycle 16). Other sequences, if present, were at levels <1 pmol after cycle 10. The appearance of the *N*-acetylglucosaminylasparagine peak in cycle 16 was consistent with glycosylation of γAsn-141 sensitive to Endo H. Tic marks on the vertical axis represent 1 mV. Mass levels detected in cycles 15 and 16 for PTH−Asp were 5.1 and 4.6 pmol, respectively, and for PTH−Asn, 3.9 and 4.5 pmol.

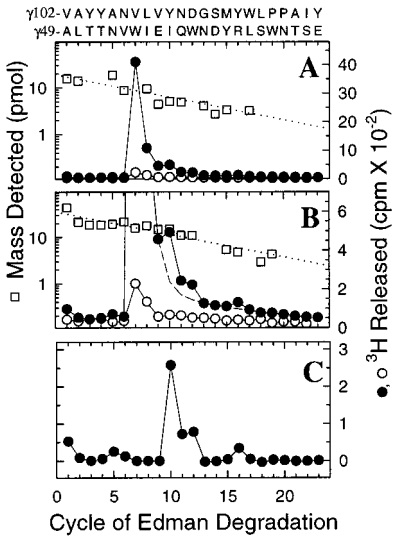

FIGURE 4: Amino-terminal sequence analysis of 14 kDa [^{3}H]dTC-labeled nAChR γ-subunit fragments produced by V-8 protease "in gel" digestion. nAChR-rich membranes (10 mg, 9 nmol of ACh-binding sites) were photolabeled with 900 nM [^{3}H]dTC (±Carb) and fractionated by SDS−PAGE. The gel piece containing the γ-subunit was excised and transferred to a 15% acrylamide mapping gel for digestion with 200 μg of V8 protease as described in Methods and ref *14*. γV8−14 was isolated from the gel with specific activities of 2120 cpm/μg (−Carb) and 290 cpm/μg (+Carb), and aliquots were sequenced. (A and B) ^{3}H release profiles from 23 cycles of Edman degradation (●, −Carb, 31 000 cpm loaded, 8900 left on the filter; ○, +Carb, 10 000 cpm loaded, 2200 left on filter) with Panel B a magnification of the ^{3}H release profile to highlight release beyond cycle 7. For the −Carb sample, three γ-subunit fragments were present: γAla-49 (I = 18 pmol, R = 89%, □ in panel A), γVal-102 (I = 27 pmol, R = 92%, □ in panel B), and γLeu-373 (I = 37 pmol, R = 89%, data not shown). The dotted lines (⋯) represent best fits of the mass values from the γAla-49 (A) and γVal-102 (B) peptides, calculated as described in Methods. The three fragments were present at similar mass levels in the +Carb sample (not shown). Release of ^{3}H in cycle 7 (4000 cpm) results from [^{3}H]dTC incorporation into γTrp-55 (335 cpm/pmol). In Panel B, the dashed line (- - -) represents a calculated second-order decay function fit to the ^{3}H release in cycles 7−9 that estimates the portion of ^{3}H release detected after cycle 7 attributable to γTrp-55 incorporation. (C) Calculated ^{3}H cpm release determined as the difference between the observed ^{3}H release at each cycle and the decay function plotted in B for ^{3}H release after cycle 7 attributable to γTrp-55. Release of ^{3}H was additionally and reproducibly detected in the 10th and 16th cycles (260 and 34 cpm, respectively). If this release is from the γVal-102 peptide, then the specific activities of [^{3}H]dTC incorporation into γTyr-111 and γTyr-117 were 15 and 3 cpm/pmol, respectively.

of the fact that Endo H removes all but the last *N*-acetylglucosamine connected to the asparagine, leaving a unique amino acid whose PTH derivative can be detected in the sequencer chromatogram (ref *31* and Figure 3B). The presence of the PTH derivative of *N*-acetylglucosaminyl-asparagine in place of PTH-asparagine in cycle 16 (Figure 3C) established that γAsn-141 was glycosylated and that its carbohydrate is Endo H-sensitive. This finding was consistent with [^{3}H]dTC labeling of γTyr-111 and γTyr-117: The ^{3}H-labeled γ-subunit fragment beginning at γVal-102 that was generated by V8 protease must contain γAsn-141, since there are no V8 protease cleavage sites (glutamic acids) between γVal-102 and γAsn-141.

In contrast to the results described above for solution digests of γ-subunit with V8 protease, analysis of the [^{3}H]-dTC incorporation in γ-subunit when V8 protease was used in conjunction with an "in gel" digestion strategy (see methods) revealed that the *primary* ^{3}H incorporation was located at the seventh cycle of Edman degradation after a V8 protease cleavage site at γGlu-48 (ref *14* and Figure 4). Even though the γVal-102 peptide was present at a mass level similar to that of the fragment beginning at γAla-49, the release of ^{3}H at cycles 10 (γTyr-111) and 16 (γTyr-117) was obscured by the overwhelming ^{3}H release at cycle 7 (γTrp-55). Calculations of the efficiency of [^{3}H]dTC photoincorporation into these three positions indicate that γTyr-111 and γTyr-117 are labeled at ~5% and 1% of the efficiency of γTrp-55, respectively.

γTyr-111 Mutational Analysis. Alignment of the *Torpedo* nAChR γ- and δ-subunit sequences in the region around γTyr-111 identified δArg-113 and δThr-119 as the residues corresponding to γTyr-111 and γTyr-117, respectively. γTyr-111 was positioned close enough to the high-affinity dTC-binding site to incorporate [^{3}H]dTC, and if δArg-113 was positioned similarly within the low-affinity dTC-binding site,

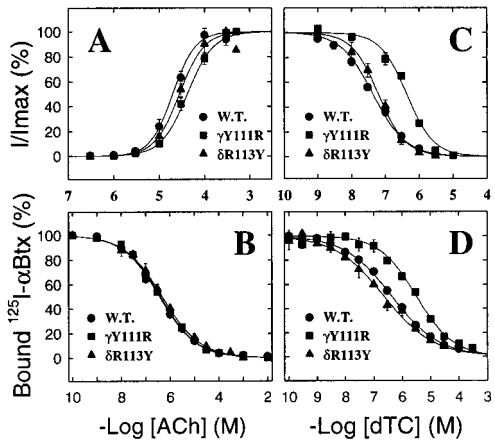

FIGURE 5: Functional consequences of γY111R (γ^m) and δR113Y (δ^m) mutations. For wild-type (●), $\alpha_2\beta\gamma^m\delta$ (■), or $\alpha_2\beta\gamma\delta^m$ (▲) nAChRs expressed in *Xenopus* oocytes, the concentration dependence of ACh-induced currents (A) and of the dTC inhibition of ACh currents (C) was determined by a two-electrode voltage clamp, and the equilibrium binding of ACh (B) and of dTC (D) was determined from their inhibition of [^{125}I]αBtx binding to receptors in membranes isolated from oocyte homogenates. (A) For ACh, the concentrations for half-maximal responses (K_{ap}) were similar for wild-type ($K_{ap} = 20 \pm 2$ μM, $N = 6$ oocytes) and for nAChRs containing γ^m ($K_{ap} = 41 \pm 4$ μM, $N = 3$ oocytes) or δ^m (28 ± 2 μM, $N = 3$ oocytes) subunits. (B) The equilibrium binding of ACh was not altered by either the γY111R or δR113Y mutation. The concentration dependence of ACh inhibition of [^{125}I]αBtx binding to wild-type nAChR was characterized by $IC_{50} = 340 \pm 20$ nM and a Hill coefficient (n_H) of 0.56 ± 0.02, or when fit by the two-site model (eq 2, Methods), by $K_H = 55 \pm 1$ nM and $K_L = 3 \pm 1$ μM. ACh binding to $\alpha_2\beta\gamma^m\delta$ ($K_H = 57 \pm 1$ nM, $K_L = 3 \pm 0.3$ μM) and $\alpha_2\beta\gamma\delta^m$ ($K_H = 69 \pm 1$ nM, $K_L = 4 \pm 1$ μM) receptors was similar to wild type. (C) The γY111R mutation, but not δR113Y, decreases the potency of dTC as an inhibitor. For dTC inhibition of current responses to 3 μM ACh, for wild-type nAChRs $IC_{50} = 40 \pm 4$ nM ($n_H = 0.9 \pm 0.1$), for $\alpha_2\beta\gamma^m\delta$ receptors $IC_{50} = 440 \pm 65$ nM ($n_H = 1.1 \pm 0.2$, $N = 3$ oocytes), and for $\alpha_2\beta\gamma\delta^m$ receptors $IC_{50} = 64 \pm 8$ ($n_H = 1.1 \pm 0.1$, $N = 3$ oocytes). (D) γY111 and δR113 are important determinants for dTC-binding selectivity. The concentration dependence of dTC inhibition of [^{125}I]αBtx binding to wild-type nAChRs was characterized by $IC_{50} = 440 \pm 3$ nM ($n_H = 0.50 \pm 0.01$) or in the two-site model by $K_H = 50 \pm 10$ nM and $K_L = 3.9 \pm 0.7$ μM. For $\alpha_2\beta\gamma^m\delta$, $IC_{50} = 3.4 \pm 0.3$ μM ($n_H = 0.67 \pm 0.04$) or $K_H = 540 \pm 110$ nM and $K_L = 17 \pm 3$ μM. For $\alpha_2\beta\gamma\delta^m$, $IC_{50} = 230 \pm 40$ nM ($n_H = 0.50 \pm 0.04$) or $K_H = 20 \pm 6$ nM and a $K_L = 2.9 \pm 0.7$ μM. The electrophysiology data are the means (±SD) from 3 to 5 experiments, while the binding data are each from a single representative experiment with each data point the mean of three samples (±SD).

repulsive interactions between the positively charged arginine and the positive charge of dTC could weaken binding at the $\alpha-\delta$ site relative to the $\alpha-\gamma$ site. To test this hypothesis, we assayed functional properties of nAChRs expressed in *Xenopus* oocytes containing γY111R (γ^m) and/or δR113Y (δ^m) mutant subunits.

Electrophysiological Evaluation of γY111R/δR113Y Mutant nAChRs. Xenopus oocytes were injected with subunit mRNAs to express wild-type, $\alpha_2\beta\gamma^m\delta$, or $\alpha_2\beta\gamma\delta^m$ nAChR, and the concentration dependence of ACh-induced currents was determined by two electrode voltage clamp at −70 mV (Figure 5A). When the data were fit to eq 3 (Methods), K_{app} for wild-type receptor ($K_{app} = 21$ μM) was similar to that for the $\alpha_2\beta\gamma^m\delta$ receptor ($K_{app} = 41$ μM) and the $\alpha_2\beta\gamma\delta^m$ receptor ($K_{app} = 28$ μM). The Hill coefficients (n_H) determined from the slopes of plots of log current versus log-[ACh] at currents less than 20% of maximum were also similar for wild-type ($n_H = 1.8 \pm 0.1$), $\alpha_2\beta\gamma\delta^m$ ($n_H = 1.7 \pm 0.1$), and $\alpha_2\beta\gamma^m\delta$ ($n_H = 1.7 \pm 0.1$) receptors. In addition, the maximal currents observed at high ACh concentrations were similar for wild-type and mutant receptors (not shown). However, while dTC was similar in potency as an inhibitor of wild-type ($IC_{50} = 40$ nM) and $\alpha_2\beta\gamma\delta^m$ ($IC_{50} = 64$ nM) receptors, it was 10-fold less potent as an inhibitor of ACh-induced currents for the $\alpha_2\beta\gamma^m\delta$ receptor ($IC_{50} = 440$ nM) (Figure 5C).

ACh and dTC Binding to γY111R/δR113Y Mutant nAChRs. The levels of surface expression of wild-type and mutant AChRs were similar, as measured by the equilibrium binding of [^{125}I]αBtx to intact oocytes 48 h after injection of subunit mRNAs (4−6 fmol of [^{125}I]αBtx bound/oocyte). The equilibrium binding of ACh and dTC were characterized by their inhibition of [^{125}I]αBtx binding to wild-type and mutant AChRs in membranes isolated from oocyte homogenates. The concentration dependence of ACh inhibition of [^{125}I]αBtx binding was essentially the same for wild-type ($IC_{50} = 340$ nM, $n_H = 0.56$), $\alpha_2\beta\gamma^m\delta$, and $\alpha_2\beta\gamma\delta^m$ receptors (Figure 5B). The data were fit well by a two-site model with dissociation constants (K_{dH} and K_{dL}) of 55 nM and 3 μM for wild-type and similar values for $\alpha_2\beta\gamma^m\delta$ ($K_{dH} = 57$ nM, $K_{dL} = 3$ μM) and $\alpha_2\beta\gamma\delta^m$ receptor ($K_{dH} = 69$ nM, $K_{dL} = 4$ μM).

For dTC and wild-type receptor, the inhibition of [^{125}I]αBtx binding ($IC_{50} = 440$ nM, $n_H = 0.5$) was also well fit by a two-site model ($K_{dH} = 50$ nM, $K_{dL} = 4$ μM) (Figure 5D). dTC binding to the $\alpha_2\beta\gamma\delta^m$ receptor ($K_{dH} = 20$ nM, $K_{dL} = 3$ μM) was similar to that for wild-type, while for the $\alpha_2\beta\gamma^m\delta$ receptor dTC binding was weakened by 10-fold at the high-affinity site and also weakened 4-fold at the low-affinity site ($K_{dH} = 540$ nM, $K_{dL} = 17$ μM).

αCtx MI Binding to γY111R/δR113Y Mutant nAChR. The equilibrium binding of αCtx MI was measured from its inhibition of binding of [^{125}I]αBtx binding to wild-type and mutant receptors. αCtx MI binds with ∼1000-fold higher affinity to the $\alpha-\gamma$ site than to the $\alpha-\delta$ site in AChRs in *Torpedo* nAChR-rich membranes (*6*, *7*), and we found that for *Torpedo* nAChRs expressed in oocytes, equilibrium binding of αCtx MI ($K_{dH} = 8$ nM, $K_{dL} = 1$ μM) was similar to that seen for nAChRs in native *Torpedo* membranes ($K_{dH} = 2$ nM, $K_{dL} = 1$ μM) (Figure 6A). As in previous analyses of the determinants of αCtx MI selectivity for the $\alpha-\delta$ site in mouse muscle nAChR (*12*), we evaluated the effects of the γY111R and δR113Y mutations by measuring the binding of αCtx MI (and [^{125}I]αBtx) to γ-less ($\alpha_2\beta\delta_2$) and δ-less ($\alpha_2\beta\gamma_2$) mutant and nonmutant receptors expressed in oocytes (Figure 6B). The $\alpha_2\beta\gamma_2$ receptor bound αCtx M1 with high affinity ($IC_{50} = 32$ nM, $n_H = 1.0$), and the γY111R substitution weakened binding by ∼1000-fold ($\alpha_2\beta\gamma^m{}_2$, $IC_{50} = 42\,000$ nM, $n_H = 1.0$). In contrast, the $\alpha_2\beta\delta_2$ receptor bound αCtx M1 weakly ($IC_{50} = 1200$ nM, $n_H = 1.1$), and the δR113Y replacement resulted in a 1000-fold *enhancement* of affinity ($\alpha_2\beta\delta^m{}_2$, $IC_{50} = 1.6$ nM, $n_H = 0.8$).

DISCUSSION

[^{3}H]dTC Photoincorporation into γTyr-111 and γTyr-117. UV irradiation of nAChR-rich membranes equilibrated with [^{3}H]dTC results in the covalent incorporation of a small percentage (<5%) of the bound [^{3}H]dTC into the nAChR α-, γ-, and δ-subunits. Previously, we identified the primary

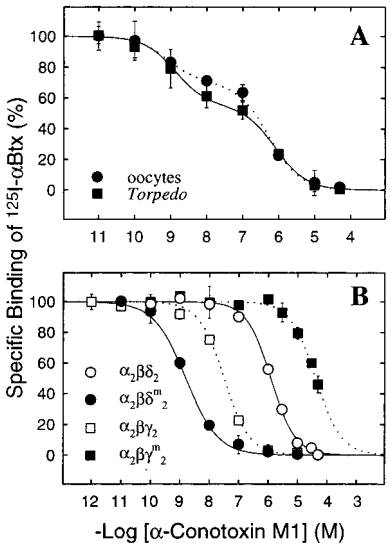

FIGURE 6: For *Torpedo* nAChR, γY111 and δR113 are the determinants for the selective binding of αCtx MI at the $\alpha-\gamma$ site. (A) Equilibrium binding of αCtx MI as determined by its inhibition of [^{125}I]αBtx binding to *Torpedo* nAChR-rich membranes (■) or to *Torpedo* $\alpha_2\beta\gamma\delta$ nAChRs in membranes isolated from oocyte homogenates (●). For the native *Torpedo* nAChR, $K_H = 1.6 \pm 1.4$ nM and $K_L = 1.0 \pm 0.3$ μM, with 50% of binding associated with the high-affinity αCtx MI site. For $\alpha_2\beta\gamma\delta$ expressed in oocytes, the data are fit by $K_H = 8 \pm 7$ nM and $K_L = 1.1 \pm 0.6$ μM, with 30% of [^{125}I]αBtx binding to the high-affinity αCtx MI site. (B) Equilibrium binding of αCtx MI to receptors lacking γ- or δ-subunit, as determined by inhibition of [^{125}I]αBtx binding. For $\alpha_2\beta\delta_2$ (○), αCtx MI binding is well fit by a single-site model ($IC_{50} = 1.2 \pm 0.1$ μM, $n_H = 1.1 \pm 0.1$). In the presence of mutant δ-subunit (δR113Y, δ^m), the binding affinity of αCtx MI to $\alpha_2\beta\delta^m{}_2$ (●) is increased 1000-fold ($IC_{50} = 1.6 \pm 0.6$ nM, $n_H = 0.8 \pm 0.1$). For $\alpha_2\beta\gamma_2$ (□), αCtx MI binds with a high affinity ($IC_{50} = 32 \pm 3$ nM, $n_H = 1.0 \pm 0.1$). With the mutant γ-subunit (γY111R, γ^m), αCtx MI binding to $\alpha_2\beta\gamma^m{}_2$ (■) is weakened by 1000-fold ($IC_{50} = 42 \pm 2$ μM, $n_H = 1.0 \pm 0.1$). Shown are the means ±SD of data from three experiments.

sites of specific [^{3}H]dTC photoincorporation (αTyr-190, γTrp-55, and δTrp-57), as well as additional amino acids in α-subunit labeled at lower efficiency (αCys-192 and αTyr-198; ref *14*). In this report we identify two additional amino acids in γ-subunit (γTyr-111 and γTyr-117) that are labeled when [^{3}H]dTC is bound to the agonist site at the $\alpha-\gamma$-subunit interface. These labeled amino acids were identified by sequence analysis of an HPLC purified fragment of γ-subunit beginning at γVal-102 (Figure 2) that was produced by subunit cleavage in solution with V8 protease. To confirm this identification, we demonstrated that the subunit fragment containing the ^{3}H-labeled amino acids also contained γAsn-141, one of the two Asn-linked glycosylation sites in the *Torpedo* nAChR γ-subunit. The identification of the labeled amino acids within the fragment beginning at γVal-102 was dependent on the more extensive digestion produced in solution compared with digestion of γ-subunit by V8 protease "in gel". Digestion "in gel" produced a fragment of 14 kDa beginning at γAla-49 that contained [^{3}H]dTC-labeled γTrp-55 as well as the fragment beginning at γVal-102 (*14*). The absence of the γAla-49 fragment from the 14 kDa band after digestion in solution probably resulted from cleavage at γGlu-57, which would generate a nonapeptide-containing [^{3}H]dTC-labeled γTrp-55 which would not have been retained in the gel.

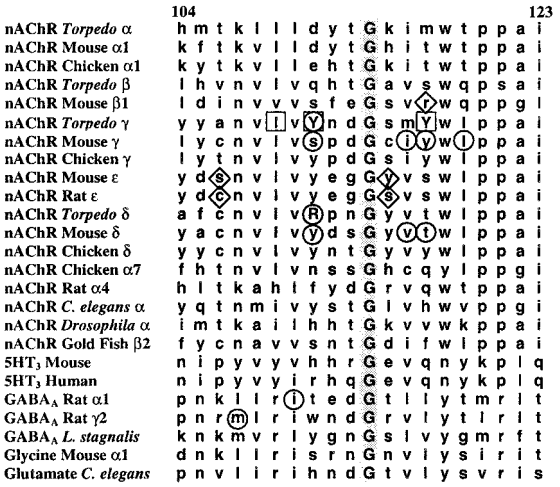

FIGURE 7: Sequence alignment of ligand-gated ion channel subunits in the region of γTyr-111/δArg-113 and γTyr-117. Representative sequences were obtained from Genbank. Accession numbers for the sequences follow in order of appearance: J00963, X03986, P09479, J00964, M14537, J00966, X03818, K02904, X55718, P09660, J00965, L10076, K02903, X68246, P09483, P48180, X07194, X54052, X79283, AJ003079, P18504, P18508, X58638, C49970, and U14524. Numbering reflects *Torpedo* α-subunit sequence of the mature protein. The glycine completely conserved in all members of the superfamily of ligand-gated ion channels is shaded: □, residues identified by photoaffinity labeling (*Torpedo* γTyr-111 and γTyr-117 (this report) and γLeu-109 (*38*)); ○, residues where mutations affect competitive antagonist binding in *Torpedo* nAChR (γTyr-111/δArg-113 (this report)) or mouse nAChR (γIle-116/δVal-118 and γTyr-117/δThr-119 (*11*), γSer-111/δThr-119 (*12*), and γLeu-119 (*37*)) or where mutations in $GABA_A$ receptors affect agonist binding (α1Ile-121 (*41*)) or benzodiazepine binding (γ2Met-130 (*42*)): ◇, residues where mutations affect assembly at subunit interfaces (mouse/rat ϵSer-106/Cys-106 and ϵTyr-115/Ser-115 (*35*) and mouse βArg-117 (*36*)).

[^{3}H]dTC photoincorporates into γTyr-111 and γTyr-117 at only 5% and 1% (respectively) of the efficiency of labeling at γTrp-55. This low relative efficiency of incorporation is unlikely to reflect the intrinsic reactivity of the tyrosine side chain, since the primary site of photoincorporation in α-subunit is also a tyrosine (αTyr-190) which incorporates [^{3}H]dTC with efficiency similar to that of γTrp-55 (*14*). Therefore, the lower efficiencies of incorporation at γTyr-111 and γTyr-117 most likely reflect differential positioning between the photoreactive center(s) in bound dTC and those tyrosines compared with γTrp-55. Unfortunately, since the photochemistry of dTC is only poorly understood, the specific spatial arrangement between γTrp-55 and the loop defined by γTyr-111 and γTyr-117 cannot be determined from these experiments alone.

Our lack of understanding of dTC photochemistry does not totally prevent structural predictions based upon our affinity-labeling results. Amino acid sequence alignment of the superfamily of ligand-gated ion channels identifies a conserved glycine residue between γTyr-111 and γTyr-117; γGly-114 (Figure 7). The complete conservation of a residue such as Gly-114 in an extended super-family of homologous proteins (>150 sequences) with representatives of 5 receptor types (ACh, GABA, glycine, serotonin, and glutamate) from four animal phyla (Chordata, Arthropoda, Mollusca, and Nematoda (*32*)) would indicate importance in structure, function, and/or expression. Glycine residues are commonly found within loops since their lack of side chain allows for

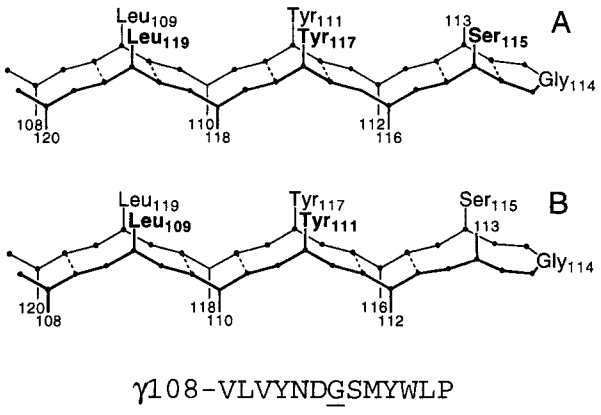

FIGURE 8: *Torpedo* γ108−120 in antiparallel β-sheets with either a γ-turn or a three-residue turn around γGly-114 orients on a common surface amino acids contributing to binding site subunit interface. (A) A γ-turn around Gly-114 requires one or two hydrogen bonds between the amines and the carboxyl oxygens of residues 113 and 115 (dotted lines). (B) A three-residue loop would require hydrogen bonds between the amines and the carboxyl oxygens of residues 112 and 116. In addition to the tightness of the turns, a γ-turn hairpin loop would differ from a three-residue hairpin loop in the direction of the turn (as shown), due to the chirality of the amino acids. An antiparallel β-sheet structure places on a common surface the side chains identified within the agonist site by affinity labeling (γ109, 111, and 117), site-directed mutagenesis (γ111/δ113 and γ117/δ119 (*11*, *12*)), and cysteine modification (γ119 (*37*)). Additionally, side chains identified by site-directed mutagenesis as determinants of subunit assembly (ϵ115 and β117 (*35*, *36*)) are also on the same surface.

close packing of residues (*33*). dTC's proximity to 2 tyrosines equidistant from a conserved glycine suggests a hairpin loop structure which would place the two tyrosines adjacent to each other in associated antiparallel β-strands (Figure 8). The hairpin loop would require a classical γ-turn around γGly-114 (Figure 8A) or a more loosely packed 3-residue turn (Figure 8B), since the more common 2-residue β-turn would place the two tyrosines on opposite faces of the β-sheet with only one in contact with dTC. The strict conservation of the glycine residue suggests a γ-turn, since glycines are favored in tighter loops (*33*) and glycines can most easily accommodate the restricted main-chain dihedral angles necessary for classical γ-turns (*34*).

Modeling the nAChR subunit primary structure around Gly-114 as a hairpin loop is consistent with other results concerning this region. Gu et al. (*35*) identified residue 115 in the ϵ-subunits of mouse and rat as an important determinant for subunit assembly, a result suggesting that this position is exposed at the interface of subunits. In another mutational analysis of subunit assembly determinants, Kreienkamp et al. (*36*) also suggested an interface orientation for mouse β-117. Mutations of mouse nAChR γ-117 or γ-111 affected competitive antagonist affinities (*11*, *12*), while modification of a cysteine substituted at γ-119 inhibited [^{125}I]α-Btx binding (*37*). Additionally, the competitive antagonist [^{3}H]-4-benzoylbenzoylcholine specifically photoincorporates into γLeu-109 (*38*). Although γ-116 was also implicated as a minor determinant of competitive antagonist-binding affinity (*11*), the majority of these studies suggests a conserved β-sheet orientation with the side chains of residues 109 and 111 as well as 115, 117, and 119 (*Torpedo* γ-subunit numbering) facing the surface at the interface between subunits (for all subunits) and in the agonist-binding site (for γ-, δ-, and ϵ-subunits). Clearly further experimental work is required to determine whether this model of antiparallel β-strands around a γ-turn at the conserved glycine is more accurate than an alternative structural model (*3*) of this region based upon homology with the solved crystal structures of plastocyanin and pseudoazurine, proteins which do not have a conserved glycine at that position.

Functional Properties of γTyr-111/δArg-113 Substitutions. Since [^{3}H]dTC photolabeling had identified two regions of γ- (and δ-) subunit primary structure contributing to the binding sites and therefore possibly important for ligand binding, it was likely that one (or both) of these regions could contribute to the nonequivalent binding seen for dTC and many other competitive antagonists. The primary sites of [^{3}H]-dTC labeling in γ- and δ-subunits were homologous tryptophans that could not be the cause of binding affinity differences between the two agonist sites. Sequence alignment of the region including γTyr-111 and γTyr-117 (Figure 7) identified an arginine (δ113) and a threonine (δ119) as the residues within the δ-subunit primary sequence aligning with γTyr-111 and γTyr-117, respectively. Since the primary structure of this region is well-conserved in muscle nAChR subunits (Figure 7), including the glycine at residue 114 that is conserved absolutely in this superfamily of ligand-gated ion channels, the secondary and tertiary structures in this region may be conserved as well. Therefore, in *Torpedo* nAChR δArg-113 is likely to occupy a position in the $\alpha-\delta$ site equivalent to that occupied by γTyr-111 in the $\alpha-\gamma$ site. The presence of a positively charged residue could have a large effect on the binding of positively charged ligands, which includes ACh and all agonists, as well as dTC and many competitive antagonists. Interestingly, for vertebrate γ-, δ-, and ϵ-subunits, *Torpedo* δArg-113 and human δHis-114 are the only positively charged side chains between positions 108 and 120. We therefore investigated the functional consequences of this Tyr-Arg substitution in the *Torpedo* nAChR.

Neither of the mutations (γY111R or δR113Y) affected either ACh-binding affinity or the concentration dependence of channel activation in the *Torpedo* nAChR expressed in *Xenopus* oocytes. Thus, there is no evidence that this position interacts directly with ACh or is involved energetically in any of the agonist-induced conformational changes associated with gating. In contrast, the placement of a positively charged arginine residue (γY111R) within the high-affinity dTC-binding site weakened dTC binding by 10-fold, consistent with the hypothesis that interactions with this position do contribute to the differences in dTC binding at the 2 sites in *Torpedo* nAChR. Thus, for dTC, site selectivity in the *Torpedo* nAChR involves an important contribution from a position near, but distinct from, the amino acids in mouse nAChR (γIle-116, γTyr-117) that confer, along with γSer-161, the differences in dTC affinity (and which align with δVal-118, Thr-119, and Lys-163 (*11*)). This difference between species is understandable, since the only charged residue identified in the mouse nAChR study, δLys-163, aligns with an uncharged methionine in the *Torpedo* nAChR δ-subunit, while *Torpedo* δArg-113 aligns with an uncharged tyrosine in mouse δ-subunit. Further studies are required to identify other positions in *Torpedo* γ- and δ-subunits that account for the full 200-fold difference in affinity seen for dTC binding at the two sites, positions that may or may not

be the same as those identified in mouse γ- and δ-subunits.

By far the most prominent effect noted from these mutations involved αCtx MI binding. As in previous analyses of the determinants of αCtx MI selectivity for the $\alpha-\delta$ site in mouse muscle nAChR (*12*), we used γ-less ($\alpha_2\beta\delta_2$) and δ-less ($\alpha_2\beta\gamma_2$) nAChRs to characterize the effects of the amino acid exchange on αCtx M1 binding. For the γY111R mutation, a 1000-fold decrease in αCtx MI-binding affinity was observed between $\alpha_2\beta\gamma_2$ and $\alpha_2\beta\gamma^m{}_2$ nAChRs, equivalent to a decrease in the free energy of binding of ~4 kcal/mol as a consequence of a single amino acid substitution. Conversely, for $\alpha_2\beta\delta_2$ receptors the δR113Y mutation resulted in a 1000-fold *increase* in αCtx MI affinity. Thus, in *Torpedo* nAChR the residues γTyr-111 and δArg-113 are the major determinants of the difference in binding affinities between the two agonist sites for αCtx MI. However, since αCtx MI binds with 10-fold higher affinity to $\alpha_2\beta\delta^m{}_2$ than to $\alpha_2\beta\gamma_2$, and with 10-fold lower affinity to $\alpha_2\beta\gamma^m{}_2$ than to $\alpha_2\beta\delta_2$, there are presumably other positions that also contribute to the differences in αCtx MI binding at the two sites. In mouse nAChR, unlike *Torpedo*, αCtx MI binds with 10000-fold higher affinity at the $\alpha-\delta$ site, and mouse γSer-111/δTyr-113 was also identified as a binding determinant with the δY113S subunit in mouse $\alpha_2\beta\delta^m{}_2$ weakening binding by about 10-fold (*12*). However, contributions from two other positions were also required to account for the affinity differences between the two sites (γLys-34 and γPhe-172, which align with δSer-36 and δ Ile-178). The corresponding positions in *Torpedo* are γLys-34/δSer-36 and γHis-172/δIle-178. In mouse the positive charge at γLys-34 has a much less prominent repulsive effect than *Torpedo* δArg-113. The δS36K substitution in mouse $\alpha_2\beta\delta_2{}^m$ weakens binding by only 5-fold, but when combined with the δI178F substitution that on its own is energetically neutral, binding is weakened by 1000-fold.

A recent study by Hann et al. (*39*) identified Arg-9 from αCtx GI as the single residue in that toxin responsible for affinity differences between binding sites of *Torpedo* nAChR. When Arg-9 was replaced by proline, the selectivity between agonist sites was abolished. αCtx GI and αCtx MI are similar in their binding affinities at each of the *Torpedo* nAChR sites (*6*), and they are highly homologous:

αCtx GI:	ECCNP ACG**R**H YSC	(Acc # P01519)
αCtx MI:	G RCCHP ACG**K**N YSC	(Acc # P01521)

Notably, the position occupied by Arg-9 in αCtx GI also contains a positively charged residue in αCtx MI (Lys-10). It is thus likely that Lys-10 of bound αCtx MI has direct interactions with γTyr-111 and δArg-113 in the *Torpedo*-binding sites, and that repulsive interactions between the positive charges are responsible for the 1000-fold weaker binding seen at the *Torpedo* $\alpha-\delta$-binding site. Further quantitative studies of the binding energetics seen for pairs of mutant αCtx M1 and nAChRs with mutant γ- or δ-subunits will be necessary to prove the existence of such direct interactions, as has been done for the α-neurotoxin of *Naja mossambica* and residues in mouse muscle nAChR α-subunit (*9*).

The results presented in this report, in conjunction with mutational analyses of mouse muscle nAChR γ- and δ-subunits, establish that *Torpedo* γY111/δR113, or amino acids at this position or nearby in the primary structure of the mouse subunits, contribute to the structure of the agonist-binding sites and are important determinants of the binding affinities of small molecule and peptide antagonists. For *Torpedo* or mouse muscle nAChRs (*40*), amino acids in this region of primary structure are not important determinants for agonist recognition. This region of primary structure is also likely to be within the agonist-binding site for other members of this family of ligand-gated ion channels. For $\alpha1\beta2\gamma2$ $GABA_A$ receptors, α1Ile-121, which aligns with *Torpedo* α-110 (Figure 7), is a determinant of agonist gating and binding (*41*), while γ2Met-130, which aligns with *Torpedo* α-107, is important for the interactions of ligands at the benzodiazepine-binding site (*42*). For serotonin 5-HT_3 receptors, it is known that dTC binds with nanomolar affinity to the mouse receptor but 1000-fold more weakly to the human receptor that possesses 95% sequence identity (*43*), and it will be of interest to determine whether the origin of that difference is the substitution of an arginine in the human sequence for a histidine in mouse at the position equivalent to *Torpedo* γTyr-111/δArg-113.

ACKNOWLEDGMENT

We would like to thank Dr. Manjunath K. Ramarao for his assistance with the structural modeling program and Megan B. Pratt for helpful discussions.

REFERENCES

1. Karlin, A., and Akabas, M. H. (1995) *Neuron 15*, 1231−1244.
2. Hucho, F., Tsetlin, V. I., and Machold, J. (1996) *Eur. J. Biochem. 239*, 539−557.
3. Tsigelny, I., Sugiyama, N., Sine, S. M., and Taylor, P. (1997) *Biophys. J. 73*, 52−66.
4. Unwin, N. (1998) *J. Struct. Biol. 121*, 181−190.
5. Neubig, R. R., and Cohen, J. B. (1979) *Biochemistry 18*, 5464−5475.
6. Hann, R. M., Pagan, O. R., and Eterovic, V. A. (1994) *Biochemistry 33*, 14058−14063.
7. Groebe, D. R., Dumm, J. M., Levitan, E. S., and Abramson, S. N. (1995) *Mol. Pharmacol. 48*, 105−111.
8. Blount, P., and Merlie, J. P. (1989) *Neuron 3*, 349−357.
9. Ackermann, E. J., Ang, E. T. H., Kanter, J. R., Tsigelny, I., and Taylor, P. (1998) *J. Biol. Chem. 273*, 10958−10964.
10. Sugiyama, N., Marchot, P., Kawanishi, C., Osaka, H., Molles, B., Sine, S. M., and Taylor, P. (1998) *Mol. Pharmacol. 53*, 787−794.
11. Sine, S. M. (1993) *Proc. Natl. Acad. Sci. U.S.A. 90*, 9436−9440.
12. Sine, S. M., Kreienkamp, H. J., Bren, N., Maeda, R., and Taylor, P. (1995) *Neuron 15*, 205−211.
13. Pedersen, S. E., and Cohen, J. B. (1990) *Proc. Natl. Acad. Sci. U.S.A. 87*, 2785−2789.
14. Chiara, D. C., and Cohen, J. B. (1997) *J. Biol. Chem. 272*, 32940−32950.
15. Cohen, J. B., Sharp, S. D., and Liu, W. S. (1991) *J. Biol. Chem. 266*, 23354−23364.
16. Dennis, M., Giraudat, J., Kotzyba-Hibert, F., Goeldner, M., Hirth, C., Chang, J.-Y., Lazure, C., Chrétien, M., and Changeux, J.-P. (1988) *Biochemistry 27*, 2346−2357.
17. Galzi, J. L., Revah, F., Black, D., Goeldner, M., Hirth, C., and Changeux, J.-P. (1990) *J. Biol. Chem. 265*, 10430−10437.
18. Czajkowski, C., and Karlin, A. (1995) *J. Biol. Chem. 270*, 3160−3164.
19. O'Leary, M. E., Filatov, G. N., and White, M. M. (1994) *Am. J. Phys. 266*, C648−C653.
20. Xie, Y., and Cohen, J. B. (1995) *Biophys. J. Abs. 68*, A406.

21. Middleton, R. E., and Cohen, J. B. (1991) *Biochemistry 30*, 6987−6997.
22. Loring, R. H., and Schulz, D. W. (1993) *Methods Neurosci. 12*, 324−341.
23. Cleveland, D. W., Fischer, S. G., Kirschner, M. W., and Laemmli, U. K. (1977) *J. Biol. Chem. 252*, 1102−1106.
24. White, B. H., and Cohen, J. B. (1992) *J. Biol. Chem. 267*, 15770−15783.
25. Schägger, H., and von Jagow, G. (1987) *Anal. Biochem. 166*, 368−379.
26. Brauer, A. W., Oman, C. L., and Margolies, M. N. (1984) *Anal. Biochem. 137*, 134−142.
27. Czajkowski, C., Kaufmann, C., and Karlin, A. (1993) *Proc. Natl. Acad. Sci. U.S.A. 90*, 6285−6289.
28. Trimble, R. B., and Maley, F. (1984) *Anal. Biochem. 141*, 515−522.
29. Tarentino, A. L., Gomez, C. M., and Plummer, T. H., Jr. (1985) *Biochemistry 24*, 4665−4671.
30. Nomoto, H., Takahashi, N., Nagaki, Y., Endo, S., Arata, Y., and Hayashi, K. (1986) *Eur. J. Biochem. 157*, 233−242.
31. Paxton, R. J., Mooser, G., Pande, H., Lee, T. D., and Shively, J. E. (1987) *Proc. Natl. Acad. Sci. U.S.A. 84*, 920−924.
32. Chiara, D. C. (1996) *Structural studies of the nicotinic acetylcholine receptor, a ligand-gated ion channel*, Ph.D. Thesis Washington University, St. Louis, MO.
33. Kwasigroch, J.-M., Chomilier, J., and Mornon, J.-P. (1996) *J. Mol. Biol. 259*, 855−872.
34. Milner-White, E. J., Ross, B. M., Ismail, R., Belhadj-Mostefa, K., and Poet, R. (1988) *J. Mol. Biol. 204*, 777−782.
35. Gu, Y., Camacho, P., Gardner, P., and Hall, Z. W. (1991) *Neuron 6*, 879−887.
36. Kreienkamp, H. J., Maeda, R. K., Sine, S. M., and Taylor, P. (1995) *Neuron 14*, 635−644.
37. Sine, S. M. (1997) *J. Biol. Chem. 272*, 23521−23527.
38. Wang, D., Xie, Y., and Cohen, J. B. (1996) *Biophys. J. Abs. 70*, A76.
39. Hann, R. M., Pagan, O. R., Gregory, L. M., Jacome, T., and Eterovic, V. A. (1997) *Biochemistry 36*, 9051−9056.
40. Prince, R. J., and Sine, S. M. (1996) *J. Biol. Chem. 271*, 25770−25777.
41. Westh-Hansen, S. E., Rasmussen, P. B., Hastrup, S., Nabekura, J., Naguchi, K., Akaike, N., Witt, M.-R., and Nielsen, M. (1997) *Eur. J. Pharmacol. 329*, 253−257.
42. Buhr, A., and Sigel, E. (1997) *Proc. Natl. Acad. Sci. U.S.A. 94*, 8824−8829.
43. Belelli, D., Balcarek, J. M., Hope, A. G., Peters, J. A., Lambert, J. J., and Blackburn, T. P. (1995) *Mol. Pharmacol. 48*, 1054−1062.

BI9901735